Available online at www.sciencedirect.com
SCIENCE DIRECT
Catalysis Today 109 (2005) 128–134
CATALYSIS TODAY
www.elsevier.com/locate/cattod

Modelling of hydrodesulfurization catalysts II. Effects of catalyst pore structures on deactivation by metal deposits

L.O. Oyekunle *, O.B. Ikpekri, A. Jaiyeola

Department of Chemical Engineering, University of Lagos, Lagos, Nigeria

Available online 7 October 2005

Abstract

A mathematical model, previously developed to describe deactivation by metal deposition, has been applied to catalyst with macro-, micro- and random pore structures. Simulation results showed that effectiveness factor reduces progressively with the increasing age of the catalyst. For the macropore system, catalyst lifetime was found to be over 1 year and it is the highest in comparison with both micropore and random pore models. It was revealed that a pore structure in which the pore diameter is enlarged increases hydrodemetallization activity and will be very effective for improving metal resistance because pore-mouth plugging can be curtailed. Predicted catalyst lifetimes matched plant data very closely. The need to develop catalysts of optimum pore structure to achieve desirable goals has been validated.

Keywords: Modelling; Catalyst deactivation; Hydrodemetallization; Metal deposition; Pore plugging

1. Introduction

Hydrodesulfurization (HDS) processes are common and commercially proven in modern day refineries. These catalytic processes have two defined roles: desulfurization to supply low-sulfur fuel oils and pretreatment of feed residua for residuum fluid catalytic cracking. The main goal is the removal of sulfur, metals and nitrogen from residua and other heavy feedstocks. Speight [1] has given an outline of different hydroconversion processes of heavy feedstocks that have evolved during the past few decades.

Crude oils typically contain trace amounts of metals with vanadium and nickel being the most abundant. During the refining processes they become concentrated in the residual fractions and often cause severe corrosion problems with high temperature metal surfaces in steam generators. Metal also tend to form particulate emissions thereby causing air pollution. Trace metals such as nickel and vanadium negatively affect catalyst activity. Hence a preliminary stage of feedstock hydrodemetallization (HDM) prevents poison of the catalyst required for HDS [1–4].

Hydrodemetallization is the process of removing both vanadium and nickel present in the heavy oil fractions. The most commonly used materials are Ni/Mo and Co/Mo sulfided catalysts on alumina support. The support can be manufactured in a variety of shapes or may even be crushed to particles of the desired size [1]. The surface area of the catalyst is usually large (200–300 m^2/g), but almost the entire surface is contained within the pore space of the alumina. The metals Co, Mo and Ni are dispersed in a thin layer within the pore system of the alumina to form active sites. The HDM catalysts are frequently deactivated and the main cause of deactivation is the blocking and plugging of pores by metal sulfide deposits (mainly of Ni and V) and by coke formation over a period of months resulting in frequent catalyst replacements with the resultant huge costs [1,2]. Increasing the hydrogen pressure can reduce coke formation while the coke deposits are burnt off during catalyst regeneration. However, the steady deposition and gradual accumulation of metal sulfides cause irreversible catalyst deactivation and at a certain point in time so much metal has been deposited that regeneration is no longer effective. This problem can be minimized by the careful selection of HDM catalysts, reactor design and catalyst design.

The deactivation of HDS/HDM catalysts has been fairly extensively studied and a recent international symposium (ISAHOF 2004) has also covered in some depth most aspects of the subject [4]. The catalysts are normally used as extrudates or porous pellets. The particle size and pore geometry, both have an important influence on process design especially for heavy oil fractions, because large reactant molecules containing

* Corresponding author. Tel.: +234 545 4891 5x1830

0920-5861/$ – see front matter
doi:10.1016/j.cattod.2005.08.012

Nomenclature

C	instantaneous concentration of reactant
C_M	instantaneous concentration of reactant for the macropore system
C^0	initial concentration of reactant for the random pore system (kmol/m^3)
C_M^0	initial concentration of reactant for the macropore pore system (kmol/m^3)
D	bulk diffusivity
D_e	effective diffusivity
D_{em}	effective diffusivity for the micropore system
D_{eM}	effective diffusivity for the macropore system
D_m	bulk diffusivity for the micropore system
D_M	bulk diffusivity for the macropore system
D_{rM}	restricted diffusivity for the macropore system
E_m	microregion void fraction
E_M	macroregion void fraction
K	reaction rate constant per unit surface area
K_M	deposition velocity defined by Eq. (24)
L	half pore length (m)
M_{ms}	molecular weight of metal sulfide deposit
M_M	metal deposits in the macropores
r_M	instantaneous macropore radius (m)
r_r	radius of reactant molecule (m)
r_0	initial pore radius (m)
$\bar{r}$	mean random pore radius (m)
$\bar{r}_m$	mean micropore radius (m)
$\bar{r}_M$	mean macropore radius (m)
R	reaction term
R_v	reaction rate of a single pellet
t	time element (s)
x	distance coordinate along the length of a pore

Greek symbols

α	dimensionless reactant concentration
α_m	dimensionless reactant concentration for micropore system
α_M	dimensionless reactant concentration for macropore system
β	dimensionless distance along the pore (z/L)
γ	ratio of instantaneous pore radius to the initial pore radius for random pore system
γ_m	ratio of instantaneous pore radius to the initial pore radius for micropore system
γ_M	ratio of instantaneous pore radius to the initial pore radius for macropore system
δ	metal deposition thickness (m × E−7)
ε	number of metal sulfide molecules per molecule of reactant
η	instantaneous effectiveness factor
θ	porosity
λ_M	ratio of molar to pore radius for macropore system (r_r/r_M)
ρ_{ms}	density of metal sulfide
τ_m	dimensionless time for micropore system
τ_M	dimensionless time for macropore system
τ_r	dimensionless time for restricted diffusivity random pore system
τ_{rm}	dimensionless time for restricted diffusivity micropore system.
τ_{rM}	dimensionless time for restricted diffusivity macropore system
φ_M	Thiele modulus macropore system
φ_r	Thiele modulus for random pore system with restricted diffusivity
φ_{rm}	Thiele modulus for micropore system with restricted diffusivity
φ_{rM}	Thiele modulus for macropore system with restricted diffusivity

metals can cause diffusional problems in the catalyst pores. Pore size and its distribution are the major factors to be considered in developing suitable fixed bed catalysts to achieve optimum HDM/HDS activities.

In recent years considerable attention has been paid to the study of HDM catalysts. Characterization of residue HDM catalysts with bimodal pore size distribution by Gualda and Kasztelan [5] showed that both vanadium and carbon were well distributed in the catalyst grain and a small amount of vanadium well dispersed was found to be more deactivating than a large amount of carbon. The activity of HDM catalysts was studied by Galiasso et al. [6] and vanadium deposition located in the meso-macropores produced a progressive decrease in activity as a function of time. Multilayer deposition of vanadium in pore entrances reduced the effective diffusivity and accessibility of large molecules to the interior of the catalyst particle, resulting in pore plugging. Investigation of aged HDM catalysts used for deasphalted vacuum bottoms in a commercial reactor by Nunez and Villamizar [7] showed that the retained metals in different amounts depended on their physicochemical characteristics. The active area was found to be located in pores of a minimum pore size diameter of about 104 Å. During the HDM reactions of Maya heavy crude oil studied by Ancheyta-Juarez et al. [8], it was observed that the catalyst having high pore volume in the 100–250 Å region showed high HDM activities. The optimum pore diameter for the removal of sulfur and nitrogen compounds was found smaller than that required for metals.

There is much progress in residual HDM catalyst deactivation studies and improved catalysts are being developed. Increased attention is directed at finding an optimum pore size for HDM catalysts and this depends on the quality of the feedstocks. The present investigation is aimed at applying a previously developed model to determine the effect of macro-, micro- and random pore structures on HDM catalysts [9–13].

2. Model formulation and description

2.1. Main assumptions

All the major assumptions made have been presented elsewhere [11,12]. The heterogeneous catalyst system was

made up of solid material with straight cylindrical pores through which the reactants and products diffuse. In the random pore model the pellet pore size distribution is broken into macropore and micropore structures and often a pore radius of about 100 Å is used as the dividing point. The active area for metallic molecules has been found to be located in pores of a minimum pore diameter of 104 Å [7], while the molecular sizes of the reacting species range from about 25 to 150 Å [14].

Catalysts used in distillate HDS applications generally possess porous structures with much of their pore volume in pores less than 100 Å, while most residual HDS/HDM catalysts are more concentrated in the region of 100–250 Å (about 70 vol.%) [15,16].

In the present model it is assumed that the HDS reaction occurs in series in both pores and there are interconnections between the macro and micropores. An idealized pore model due to Wheeler [17] was applied making use of an average value for the tortuosity factor for interconnecting pores.

2.2. Further assumptions

(a) Mass transfer limitation does not exist between the gas and liquid phase because hydrogen is in excess. Commercial HDM reactors operate adiabatically with a continuous gas phase, with the oil dispersed in the trickle flow regime, and with very low external diffusional gradients [18].
(b) The reactor operates at negligible pressure and temperature gradient; hence fluid flow into pores is by isothermal diffusion. Temperature homogeneity can be improved by diluting the catalyst bed with inert materials [18,19].
(c) The pores have small sizes and the flow is unidirectional and towards the pore length only.
(d) Molecules diffuse rapidly into the pores and radial concentration gradients are negligible.
(e) The HDM reaction is second order occurring at 675 K and a pressure of 200 kg/cm^2.

2.3. Reaction inside the pore

Diffusion and reaction within the pores can therefore be described by the continuity equation:

$$\frac{\partial C}{\partial t} = D\frac{\partial^2 C}{\partial z^2} + R \tag{1}$$

where D is the bulk diffusivity and R is the reaction rate.

2.4. Macropore model

When the mean pore radius is above 100 Å, transport in the pellet is said to occur in the macropore region [14,20]. Hence bulk diffusion would prevail in the pores. The effective diffusivity for macropore disperse system is given by

$$D_{eM} = D_M E_M^2 \tag{2}$$

The continuity equation for macropore system is given by

$$\frac{\partial C}{\partial t} = D_{eM}\frac{\partial^2 C}{\partial x^2} + R \tag{3}$$

For the reaction term, R,

$$R = -KC_M^2\left[\frac{\text{surface area of macropore}}{\text{volume of macropore}}\right]$$

$$R = -KC_M^2\left[\frac{2\pi\bar{r}_M L}{\pi\bar{r}_M^2 L}\right]$$

$$R = -KC_M^2\left[\frac{2}{\bar{r}_M}\right] \tag{4}$$

Eq. (3) becomes

$$\frac{\partial C_M}{\partial t} = D_{eM}\frac{\partial^2 C_M}{\partial x^2} - KC_M^2\left[\frac{2}{\bar{r}_M}\right] \tag{5}$$

In terms of dimensionless parameters:

$$\alpha_M = \frac{C_M}{C_M^0} \tag{5a}$$

$$\beta = \frac{x}{L} \tag{5b}$$

$$\tau_M = \frac{tD_{eM}}{L^2} \tag{5c}$$

$$\varphi_M = L\left[\frac{2KC_M^0}{\bar{r}_M D_{eM}}\right]^{1/2} \tag{5d}$$

Eq. (5) becomes

$$\frac{\partial^2 \alpha_M}{\partial \beta^2} = \varphi_M^2\alpha_M^2 + \frac{\partial \alpha_M}{\partial \tau_M} \tag{6}$$

with the following boundary conditions:

$$\text{at } x = 0, \quad C_M = C_M^0 \quad \text{and} \quad \alpha_M = 1, \quad \beta = 0 \tag{7}$$

$$\text{at } x = L, \quad \frac{\partial C_M}{\partial x} = 0 \quad \text{and} \quad \beta = 1 \tag{8}$$

$$\text{at } \tau_M = 0, \quad \alpha_M = 1 \tag{9}$$

2.5. Restricted diffusivity

It is well known that the rate-limiting step for HDM reaction usually is the diffusion of very large reactant molecules into the catalyst pores. Diffusion of materials in and out of the macropore is restricted by deposition of metal sulfide in the pore. The restricted diffusivity is given as:

$$D_{rM} = D_{eM}(1 - \lambda_M)^4 \tag{10}$$

where

$$\lambda_M = \frac{r_r}{r_M} \tag{11}$$

In terms of dimensionless parameters:

$$\tau_{rM} = \frac{tD_{rM}}{L^2} \tag{12}$$

$$\varphi_{rM} = L\left[\frac{2KC_M^0}{r_M D_{rM}}\right]^{1/2} \tag{13}$$

Eq. (6) becomes

$$\frac{\partial^2 \alpha_M}{\partial \beta^2} = \varphi_{rM}^2 \alpha_M^2 + \frac{\partial \alpha_M}{\partial \tau_{rM}} \tag{14}$$

with the new boundary conditions:

$$\alpha_M = 1 \quad \text{at } \beta = 0 \tag{15}$$

$$\frac{\partial \alpha_M}{\partial \beta} = 0 \quad \text{at } \beta = 1 \tag{16}$$

$$\alpha_M = 1 \quad \text{when } \tau_{rM} = 0 \tag{17}$$

The concentration profiles (α_M) for the macropore system can be obtained by solving Eq. (14). The metal deposition rate is given by

$$\frac{dM_M}{dt} = E2\pi r_M K C_M^2 M_{ms} \tag{18}$$

The metal deposition in the macropore is obtained from

$$M_M = \rho_{ms}\pi(\bar{r}_M^2 - r_M^2) \tag{19}$$

where ρ_{ms} is the density of metal sulfide deposit.

Putting $\gamma_M = \frac{r_M}{\bar{r}_M}$

$$M_M = \rho_{ms}\pi\bar{r}_M^2(1 - \gamma_M^2) \tag{20}$$

and therefore

$$\frac{dM_M}{dt} = \frac{d}{dt}[\rho_{ms}\pi\bar{r}_M^2(1 - \gamma_M^2)] = \varepsilon 2\pi r_M K C_M^2 M_{ms} \tag{21}$$

where ε is the number of sulfide molecules per molecule of reactant, and M_{ms} is the molecular weight of metal sulfide deposit.

Differentiation of (21) yields

$$\frac{d\gamma_M}{dt} = -\frac{\varepsilon K (C_M^0)^2 M_{ms}\alpha_M^2}{\rho_{ms}\bar{r}_M} \tag{22}$$

Hence

$$\frac{d\gamma_M}{dt} = -\frac{K_M \alpha_M^2}{\bar{r}_M} \tag{23}$$

where

$$K_M = -\frac{\varepsilon K (C_M^0)^2 M_{ms}}{\rho_{ms}} \tag{24}$$

with the boundary condition:

$\gamma_M = 1$ at $t = 1$.

In dimensionless terms

$$\frac{d\gamma_M}{d\tau_{rM}} = -\frac{K_M L^2 \alpha_M^2}{D_{rM}\bar{r}_M} \tag{25}$$

where $\tau_{rM} = \frac{tD_{rM}}{L^2}$ with the new boundary conditions: $\gamma_M = 1$ at $\tau_{rM} = 0$.

The metal deposition thickness is related to γ_M according to the expression

$$\delta_M = \bar{r}_M(1 - \lambda_M) \tag{26}$$

Eqs. (14) and (22) will be solved simultaneously for concentration profiles and metal deposition thickness as a function of time for macropore structure.

2.6. Micropore model

In the micropores of a catalyst pellet where the mean pore radius is below 100 Å, diffusion is predominantly Knudsen [14]. Effective diffusivity in the micropore is given by

$$D_{em} = D_m E_m^2 \tag{27}$$

Rate equations similar to those of macropore were also derived for the micropore system.

The following results were obtained:

- For concentration profiles:

$$\frac{\partial^2 \alpha_m}{\partial \beta^2} = \varphi_{rm}^2 \alpha_m^2 + \frac{\partial \alpha_m}{\partial \tau_{rm}} \tag{28}$$

with the following boundary conditions:

$$\alpha_m = 1 \quad \text{at } \beta = 0 \tag{29}$$

$$\frac{\partial \alpha_m}{\partial \beta} = 0 \quad \text{at } \beta = 1 \tag{30}$$

$$\alpha_m = 1 \quad \text{when } \tau_{rm} = 0 \tag{31}$$

- For metal deposition:

$$\frac{d\gamma_m}{dt} = -\frac{\varepsilon K (C_m^0)^2 M_{ms}\alpha_m^2}{\rho_{ms}\bar{r}_m} \tag{32}$$

Both Eqs. (28) and (32) were solved simultaneously at different time intervals.

2.7. Random pore model

In order to estimate the effective diffusivity (D_e) for the bidisperse system, the first step is to evaluate the diffusivity for single cylindrical pore sizes for both macro and microregions

and combine this with pore size distribution information. The various parallel contribution are added together [14] to give the following:

$$D_e = E_M^2 D_M + \frac{E_m^2(1+3E_M)}{1-E_M} D_m \quad (33)$$

The corresponding rate equations developed for the bidisperse system taking into consideration the effective diffusivity (D_e) were as follows:

- For concentration profiles:

$$\frac{\partial^2 \alpha}{\partial \beta^2} = \varphi_r^2 \alpha^2 + \frac{\partial \alpha}{\partial \tau_m} \quad (34)$$

with the boundary conditions:

$$\alpha = 1 \quad \text{at } \beta = 0 \quad (35)$$

$$\frac{\partial \alpha}{\partial \beta} = 0 \quad \text{at } \beta = 1 \quad (36)$$

$$\alpha = 1 \quad \text{when } \tau_r = 0 \quad (37)$$

- For metal deposition:

$$\frac{d\gamma}{dt} = -\frac{\varepsilon K (C^0)^2 M_{ms} \alpha_m^2}{\rho_{ms} \bar{r}} \quad (38)$$

Eqs. (34) and (38) were given simultaneous solutions.

2.8. Effectiveness factor and reaction rate

Catalyst effectiveness is connected to the geometry of the pores and the effectiveness factor is the ratio of the rate of reaction with and without transport limitations.

A procedure for incorporating pore size distribution in the macro and micropores for calculating effectiveness factor (η) and the reaction rate per unit volume of catalyst (R_v) for a second order reaction is available [9–12]:

$$\eta = \int_0^1 \alpha^2 \gamma \, d\beta \quad (39)$$

$$R_v = \frac{2}{r_0} \theta K (C^0)^2 \eta \quad (40)$$

Eq. (39) was solved numerically by the use of interior collocation method to yield values for the effectiveness factor, which were then substituted into Eq. (40) to compute the corresponding values of reaction rate for different pore models.

2.9. Numerical solution

The orthogonal collocation method has been proved to be useful for problems of diffusion and reaction [21]. The method of interpolating polynomials approximation was combined with orthogonal collocation with equally spaced collocation points (representing dimensionless distance along the pore) reducing the second order partial differential equation to ordinary polynomial. The resulting ordinary differential equations were numerically solved using Runge–Kutta fourth order integral scheme. The models developed for the macro-, micro- and the random pore systems were simulated by the use of computer. The program for the three models was written in BASIC computer language [12].

3. Results and discussion

The values of the parameters used were obtained from literature sources [9–12]. These are typical of those found in commercial practice and are listed in (Table 1) with the appropriate parameters.

3.1. Metal deposition along the pore and catalyst age

The three pairs of relevant equations for macropore (Eqs. (14) and (22)), micropore (Eqs. (28) and (32)) and random pore models (Eqs. (34) and (38)) were solved simultaneously for concentration profiles and metal deposition thickness as a function of dimensionless time.

The metal deposition thickness (δ) was evaluated using Eq. (26). Fig. 1 shows that deposition of metals is a function of time on stream. It is observed that metal deposition increases with the catalyst age in the order macro > random > micropores. However, the rates of deposition are different for the three pore models. The macropore model exhibits a linear relationship while the other two models are non-linear. Low metal deposition in the micropore system resulted from the fact that most of the pores had diameter small enough to exclude metal-containing reactant molecules present in the feed while large pore diameter of the macropores can accumulate more metal deposits. Consequently, catalysts with large pore diameters appeared more promising as catalyst system of long life.

Fig. 1 also demonstrates that pore size distribution of a catalyst plays an important role during metal deposition. During HDM, two extreme cases of metal deposition occur. For macropores molecules can penetrate deep into the interior of the catalyst pore whereas for micropores metal deposition occurs predominantly on the external surface. The first case

Table 1
List of parameters used in simulation

Parameter	Value
C^0 (kmol/m^2)	2×10^{-2}
D (m^2/s)	7×10^{-12}
K (m^4/kmol s)	4.3×10^{-13}
r_0 (m)	6.25×10^{-10}
θ	0.5
ρ_{ms} (kg/m^3)	3000
ε	2
E_M	0.275
E_m	0.359
M_{ms}	149.5
Catalyst specific surface area (m^2/g)	175
Reaction temperature (K)	675
Pressure (kg/cm^2)	200

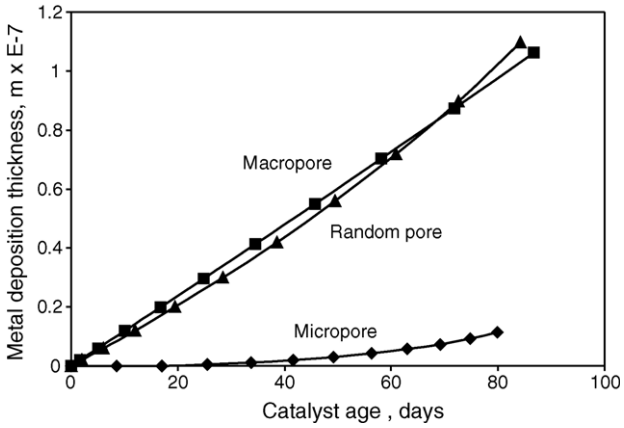

Fig. 1. Metal deposition thickness as a function of catalyst age for different pore models.

ensures that more metals can be accommodated because pore-mouth plugging is minimized. The second case leaves a large portion of the pore unused because of significant pore blockage. Metal deposition has an adverse effect on the catalyst pores since the macropores may be totally or partially blocked by metal deposits. The partially blocked macropores then become micropores. Thus, metal deposition helps to increase the percentage of micropores; Ancheyta-Juarez et al. [8,12] demonstrated that micropores with diameter less than 100 Å, exhibited a notable 300% increase in percentage of pore volume during the hydroprocessing of heavy Maya Crude.

The random pore model is a combination of micro and macro pore models in parallel. Therefore the metal deposition behavior predicted from the random pore model should be positioned between those of the other two. However, it is shown in Fig. 1 that beyond the catalyst age of 70 days, the random pore model predicts the highest metal deposition. The reason is because the mode of metal deposition depends on the pore diameter as well as the pore size distribution of the catalyst. Since the random pore model is a combination of macro and micropore models, the metal deposition thickness after about 70 days (Fig. 1) obviously shows the total sum of metal deposits as a combination of the two other models. This is quite expected as more micropores being formed from macropores of the random pore model are blocked and covered by metal deposits. Increased metal deposition of the random pore model results in lower and reduced catalyst lifetime in comparison to the macropore model.

3.2. Catalyst effectiveness

Catalyst effectiveness is closely connected to the geometry of the pores of the catalyst. Solution of Eq. (39) yielded values for instantaneous effectiveness factor (η). Fig. 2A shows that catalyst effectiveness decreases progressively with increasing pore length for the three pore structures. At pore mouth ($0 \leq \beta \leq 0.2$) of the catalyst, effectiveness factor is high and reduces rapidly as the distance along the pore increases. This trend is easily attributable to a partial blocking of the pore system by the deposited metal sulfides. Both the micropores and random pores experienced similar change in effectiveness

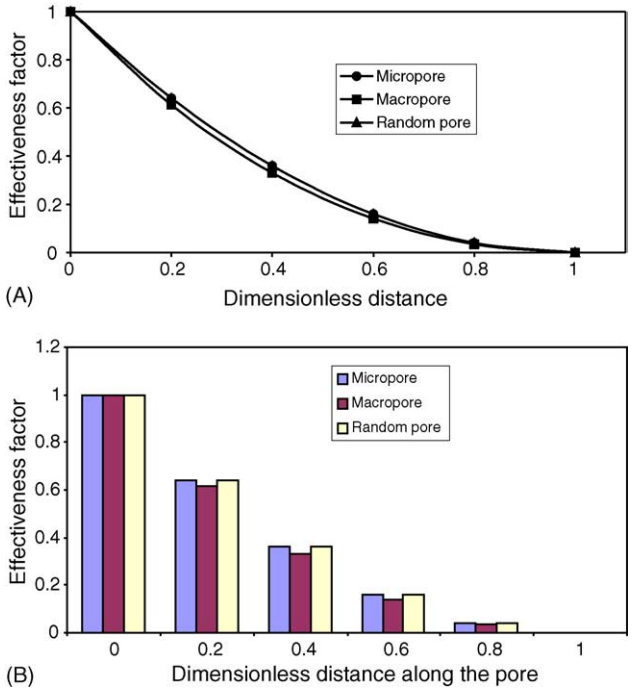

Fig. 2. (A) Variation of effectiveness factor along the pore length. (B) Block diagram of the variation of effectiveness factor with the pore length.

factor while that of the macropores was slightly different. A better picture of the variation of effectiveness factor with pore length is shown in Fig. 2B. The implication of this is that micropores contribute more to the overall pore volume in the random pore model as has been previously validated in the experimental observations of Ancheyta et al. [16].

For the different pore structures the catalyst is only effective up to about half way along the pore. This is due to the fact that metal containing compounds because of their large size do not penetrate deeply into the catalyst. They are accumulated as metal sulfides in the pore mouth of the catalyst and then block the entrance for the reactant molecules.

Fig. 3 shows the confirmation that effectiveness changes significantly during catalyst aging, which is caused by the demetallization reaction. The effectiveness factor decreases both with catalyst age and with increasing pore length indicating a high activity at the entrance of catalyst pore ($\beta = 0$). This trend is also due to the blocking of the pore mouth

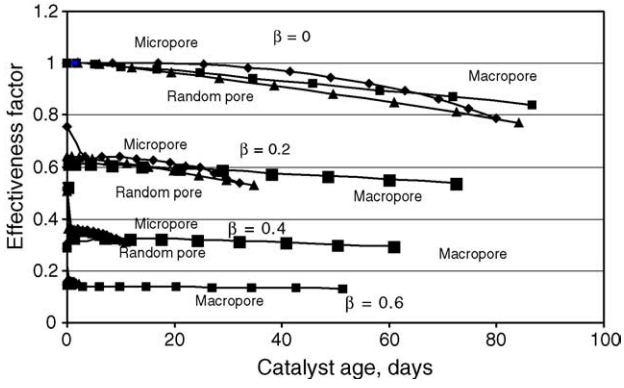

Fig. 3. Variation of effectiveness factor with catalyst age.

Table 2
Summary of life time predictions

Pore sizes	Catalyst life time, days				
	Based on effectiveness factor		Based on demetallization rate		
	This study		Previous study [10]		Previous study [12]
	Regression	Extrapolation			
Macropore	423	423	445	475	462
Micropore	141	170	95	173	150
Random pore	204	250	200	280	316

by metal deposition. A linear relationship is again reported for the macropores while there are rapid changes for both the random and micropore models. The plots clearly indicate the advantage of catalyst with macropores to provide easy access for large molecules. All the different pore systems are very effective within 5 days ($\beta = 0$) when the catalyst is still relatively fresh. The micropores recorded the highest values of effectiveness factors because micropore system has larger specific surface area (m^2/g) than the macropore [1]. This is because at $\beta = 0$ the HDM reaction occurs predominantly on the external surface when the reactant molecules have not penetrated deep into the interior of the pore and catalyst with highest surface area exhibits the highest activity. However, both the micropore and random pore models are only effective for a distance of about 50% along the pore length ($\beta = 0.4$) and only for about 40 days ($\eta = 0.2$) while the macropore is still very effective for more than 100 days. At a distance greater than 50% pore length ($\beta = 0.6$) both micropore and random pore are no longer effective but the macropore is still partially effective.

The plots recorded in Fig. 3 can be used to predict catalyst life because an effectiveness factor of 0.2 is reported reasonable for demetallization reaction [8,9]. Polynomial regression of the plots in Fig. 3 when $\beta = 0$ yields lifetimes of 141, 204 and 423 days for the micropore, random pore and macropore systems respectively while direct extrapolation produces the corresponding lifetimes of 170, 250 and 423 days. These results indicate that it is only with macropore system that catalyst can last more than 1 year.

Table 2 compares catalyst life times obtained in this study with those recorded in a previous studies [10,12] where both the rate of demetallization and the effectiveness factor were employed to determine catalyst lifetimes by assuming uniform pore plugging by metal deposition within the cylindrical pore structure. These are in agreement with catalyst lifetimes reported in the literature [1,2,9].

4. Conclusion

Modelling of catalyst deactivation during residual HDM process has been studied for different catalyst pore structures and catalyst lifetimes predicted. The study revealed that selecting an appropriate pore structure could enhance diffusion into the catalyst pores. For macropore system, catalyst lifetime is over one year and it is the longest when compared with those of the micropore and random pore models. It is concluded that mathematical models will find useful application in the design and prediction of catalyst deactivation for the purpose of optimizing plant operations.

References

[1] J.G. Speight, The Desulfurization of Heavy Oil and Residua, 2nd ed., Marcel Dekker, New York, 2000.
[2] J.G. Speight, in: J. Ancheyta, G.F. Froment (Eds.), Proceedings of the International Symposium on Advances in Hydroprocessing of Oil Fractions, ISAHOF 2004, Oaxaca, Mexico, April 18–22, 2004, pp. 61–69.
[3] N. Kagami, R. Iwamoto, T. Hirano, N. Senda, R&D on Hydrogen Treatment Technology for Long-term Continuous Operation, Copyright 2002 Petroleum Energy Center.
[4] J. Ancheyta, G.F. Froment (Eds.), Proceedings of the International Symposium on Advances in Hydroprocessing of Oil FractionsISAHOF 2004, Oaxaca, Mexico, April 18–22, 2004.
[5] G. Gualda, S. Kasztelan, J. Catal. 161 (1996) 319.
[6] R. Galiasso, R. Blanco, C. Gonzalez, N. Quinteros, Fuel 62 (1983) 817.
[7] M. Nunez, M. Villamizar, Appl. Catal. A 252 (2003) 51.
[8] J. Ancheyta-Juarez, S.K. Maity, G. Betancourt-Rivera, G. Centeno-Nolasco, P. Rayo-Mayoral, M.T. Gomez-Perez, Appl. Catal. A 216 (2001) 195.
[9] L.O. Oyekunle, R. Hughes, Chem. Eng. Res. Des. 62 (1984) 339.
[10] L.O. Oyekunle, R. Hughes, Ind. Eng. Chem. Res. 26 (1987) 1945.
[11] L.O. Oyekunle, O.B. Ikpekiri, in: J. Ancheyta, G.F. Froment (Eds.), Proceedings of the International Symposium on Advances in Hydroprocessing of Oil Fractions, ISAHOF 2004, Oaxaca, Mexico, April 18–22, 2004.
[12] L.O. Oyekunle, O.B. Ikpekiri, Ind. Eng. Chem. Res. 43 (2004) 6647.
[13] L.O. Oyekunle, B.O. Kalejaiye, Pet. Sci. Technol. 21 (2003) 1475.
[14] G.F. Froment, K.B. Bischoff, Chemical Reactor Analysis and Design, 2nd ed., John Wiley & Sons, New York, 1990, pp. 142–148.
[15] J. Ancheyta, G. Betancourt, G. Centeno, G. Marroquin, F. Alonso, Energy and Fuels 16 (2002) 1438.
[16] J. Ancheyta, G. Betancourt, G. Centeno, G. Marroquin, Energy and Fuels 17 (2003) 462.
[17] A. Wheeler, Adv. Catal. 3 (1951) 249.
[18] J. Ancheyta, G. Marroquin, M.J. Angeles, M.J. Macias, I. Pitault, M. Forissier, R.D. Morales, Energy and Fuels 16 (2002) 1059.
[19] L.C. Castañeda-Lopez, F. Alonso-Martinez, J. Ancheyta-Juarez, S.K. Maity, E. Rivera-Segundo, M.N. Matus-Guerra, Energy and Fuels 15 (2001) 1139.
[20] J.M. Smith, Chemical Engineering Kinetics, 3rd ed., McGraw-Hill, 1981.
[21] B.A. Finlayson, Nonlinear Analysis in Chemical Engineering, McGraw-Hill Inc., 1980.